



Validation of a Contour Method Single-Measurement Uncertainty Estimator

M.D. Olson¹ · A.T. DeWald¹ · M.R. Hill¹

Received: 24 October 2017 / Accepted: 12 February 2018 / Published online: 1 March 2018
© Society for Experimental Mechanics 2018

Abstract

This work validates an analytical single-measurement uncertainty estimator for contour method measurement by comparing it with a first-order uncertainty estimate provided by a repeatability study. The validation was performed on five different specimen types. The specimen types cover a range of geometries, materials, and stress conditions that represent typical structural applications. The specimen types include: an aluminum T-section, a stainless steel plate with a dissimilar metal slot-filled weld, a stainless steel forging, a titanium plate with an electron beam slot-filled weld, and a nickel disk forging. For each specimen, the residual stress was measured using the contour method on replicate specimens to assess measurement precision. The uncertainty associated with each contour method measurement was also calculated using a recently published single-measurement uncertainty estimator. Comparisons were then made between the estimated uncertainty and the demonstrated measurement precision. These results show that the single-measurement analytical uncertainty estimate has good correlation with the demonstrated repeatability. The spatial distributions of estimated uncertainty were found to be similar among the conditions evaluated, with the uncertainty relatively constant in the interior and larger along the boundaries of the measurement plane.

Keywords Residual stress measurement · Contour method · Uncertainty · Precision · Repeatability

Introduction

Experimental data and their associated uncertainty are fundamental for experimental testing, as well as for validation of engineering models. Experimental validation is the process of determining the degree to which a model is an accurate representation of the real-world from the perspective of the intended uses of the model [1] and experimental uncertainty effectively establishes the resolution at which such comparisons can be made [2]. Similarly, when experimental data are used to predict an output, the experimental data uncertainty will determine the bounds of the predicted output. The bounds of the predicted output will ultimately determine whether the experimental data are useful for predicting a real-world phenomenon. Therefore, uncertainty is important for all

measurements since it determines whether a given measurement is useful for its intended purpose.

The contour method is a residual stress measurement technique that provides a two-dimensional map of residual stress on a given measurement plane. The two-dimensional residual stress map provided by the contour method has been found to be useful for validating computation welding simulations [3–5], predicting fatigue performance [6], evaluating the effectiveness of manufacturing processes like peening [7, 8], cold hole expansion [9], and welding [10]. Although, the contour method has proven useful, most prior work lacks an uncertainty estimate for the contour method data.

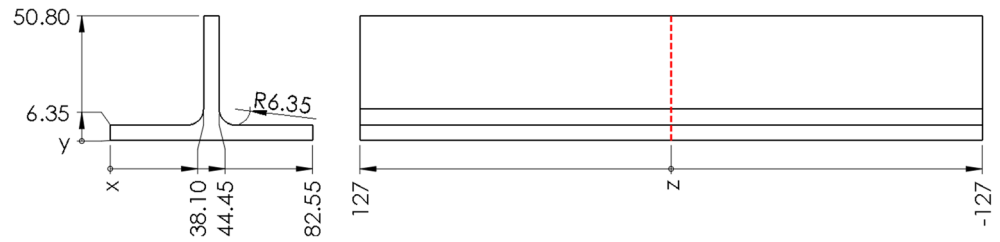
Recently, a single-measurement uncertainty estimator was developed for the contour method [11]. The objective of the present work is to validate this uncertainty estimator by assessing the level of correlation between the uncertainty estimate and a first-order uncertainty estimate. The first order uncertainty estimate is determined with a set of repeatability studies that quantify the measurement precision of the contour method over a range of conditions. Measurements were performed on specimen types that include a range of geometries, materials, and residual stress conditions. For each specimen type, the residual stress was measured on replicate specimens

✉ M. D. Olson
molson@hill-engineering.com

¹ Hill Engineering, LLC, 3083 Gold Canal Drive, Rancho Cordova, CA, USA



Fig. 1 Aluminum T-section dimensions and measurement location (dimensions in mm)



using the contour method to establish measurement precision. The single-measurement uncertainty estimate associated with each contour method measurement was also calculated. Comparisons were then made between the estimated uncertainty and the demonstrated precision to validate the uncertainty estimator.

Methods

This work includes multiple steps. First, five test specimens were designed and manufactured. The specimen types cover a range of geometry, material, and residual stress condition that represent a range of structural applications. Replicate

specimens of each type were produced (between 5 and 10 replicate specimens for each specimen type). Second, residual stress measurements were performed on each specimen type using the contour method. Third, the uncertainty associated with each single measurement was estimated. Fourth, the precision of the contour method was calculated for each specimen type. Finally, comparisons were made between the estimated uncertainty and the demonstrated precision for each specimen type. Details of the specimens, contour method, uncertainty estimation, and data comparisons follow. A more complete description of the repeatability studies can be found elsewhere [12].

Test Specimen Manufacture

Five different test specimen types were manufactured: an aluminum T-section (10 specimens), a stainless steel plate with a dissimilar metal (DM) slot-filled weld (5 specimens), a titanium plate with an electron beam (EB) slot-filled weld (6 specimens), a stainless steel forging (6 specimens), and a nickel disk forging (6 specimens).

The aluminum T-section specimen type was fabricated from 7050-T7451 aluminum plate (cut into bars) that had been stress relieved by stretching during forming. The original bars had a length of 762 mm (30.0 in), a height of 82.55 mm (3.25 in), and a width of 82.55 mm (3.25 in). The bars were heat

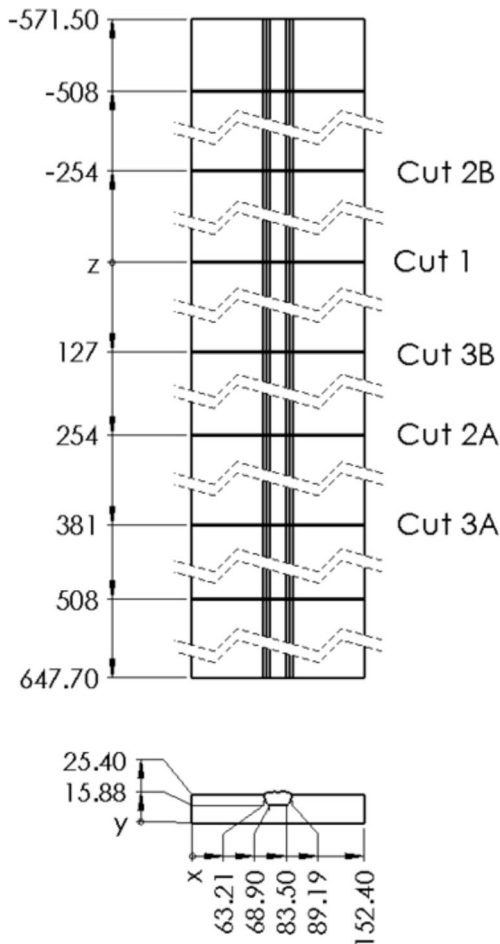


Fig. 2 Stainless steel dissimilar metal dimensions and measurement locations (dimensions in mm)

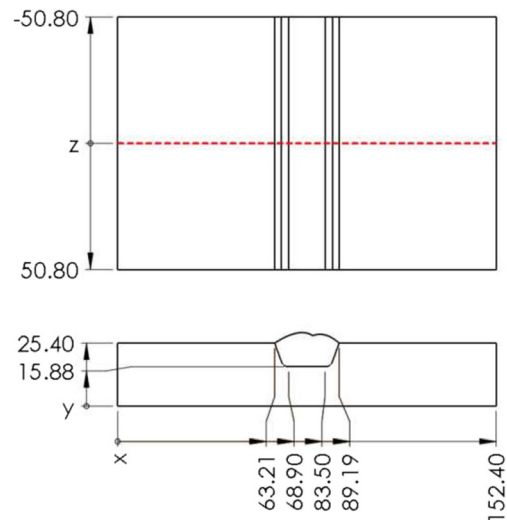


Fig. 3 Titanium electron beam welded plate dimensions and measurement location (dimensions in mm)

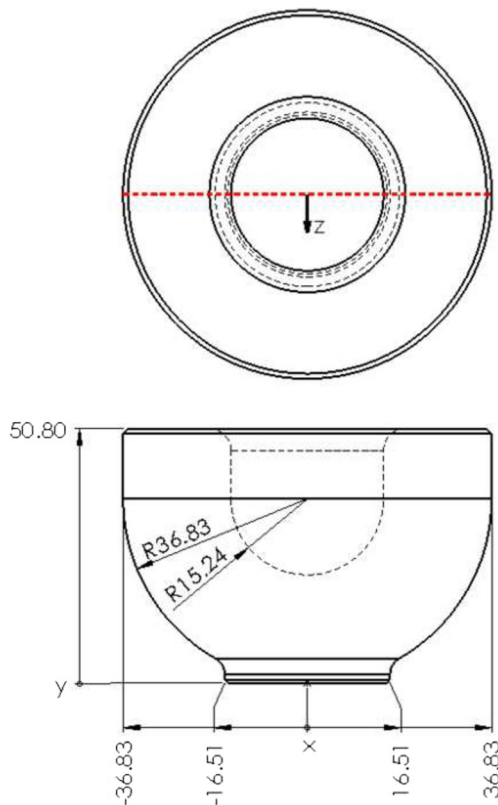


Fig. 4 Stainless steel forging dimensions and measurement location (dimensions in mm)

treated, including a quench, to induce high residual stress indicative of the -T74 temper. The heat treatment used the recipe described in [13] and consists of heating the specimens to

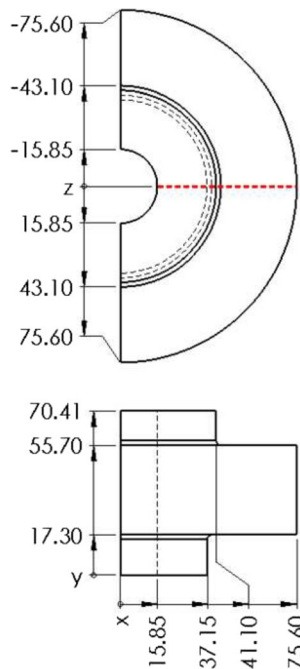


Fig. 5 Nickel disk forging dimensions and measurement location (dimensions in mm)

Table 1 Material properties for each specimen

Specimen	Elastic modulus (GPa)	Poisson's ratio	Yield strength (MPa)
Aluminum T-section (7085-T74)	71	0.33	460
Stainless steel DM welded plate (316 L plate)	203	0.3	440
Stainless steel DM welded plate (A52 weld)	211	0.289	345–482
Titanium EB welded plate (Ti-6Al-4 V)	110	0.31	960
Stainless steel forging (304 L)	200	0.249	470
Nickel disk forging (Udimet-720Li)	200	0.31	300–500

477 °C (890 °F) for 3 h, quenching in room temperature water, artificial aging at 121 °C (250 °F) for 8 h followed by additional aging at 177 °C (350 °F) for 8 h. T-sections were then machined from the bars to represent an airframe structural member. Each T-section had a length of 254 mm (10.0 in), a height of 50.8 mm (2.0 in), a width of 82.55 mm (3.25 in), and a flange thicknesses of 6.35 mm (0.25 in) as shown in Fig. 1.

The stainless steel dissimilar metal (DM) weld specimen type was fabricated from one long plate made of high-strength 316L stainless steel. The plate had a 25.4 mm (1.0 in) by 152.4 mm (6.0 in) cross-section and a length of 1.22 m (48.0 in). A slot was machined along the entire length of the plate with a 9.53 mm (0.375 in) groove depth, a 19.05 mm (0.75 in.) width, and a 70° root angle. The groove and plate cross-section can be seen in Fig. 2. Before filling in the slot with weld material, a continuous 7.94 mm (0.313 in) fillet weld was applied along the 1.22 m edges to join the plate to a stiff fixture, to add restraint during the welding process. The slot was filled with 8 passes, each applied along the entire length of the plate using an automated process and 0.89 mm (0.035 in) diameter A52M (ERNiCrFe-7A) wire. Following welding, the fillet welds were machined away to release the plate from the backing fixture and the ends of the plate were removed to eliminate the inconsistent weld bead geometry at the start and stop of the weld.

The titanium alloy electron beam (EB) welded plate specimen type was fabricated using one long plate made of Ti-6Al-4V, with similar geometry to the stainless steel DM welded plate (same cross-section and slot dimensions). The groove was filled along the entire length of the plate with 8-passes of 3.18 mm (0.125 in) diameter Ti-6Al-4V wire. After completion of the weld, the plate was sectioned into 101.6 mm (4.0 in) long pieces, as shown in Fig. 3. These specimens were representative of a typical wire fed additive manufacturing process in the as-manufactured condition (prior to thermal stress relief).

Fig. 6 (a) Measured residual stress (σ_{zz}) and (b) mean of repeatability study for the aluminum T-section specimens

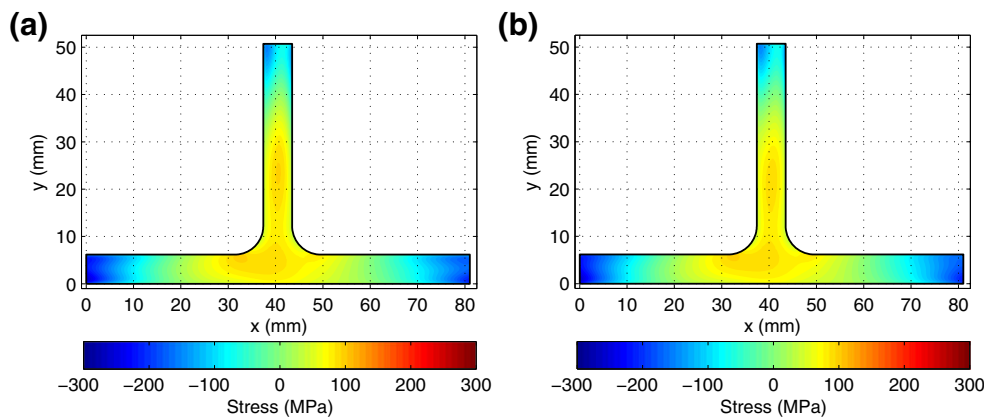


Table 2 Uncertainty and repeatability standard deviation statistical values

Specimen		Median (MPa)	Mean (MPa)	75th percentile (MPa)	95th percentile (MPa)	Max (MPa)
Aluminum T-section (7085-T74)	Uncertainty	9.9	12.1	11.9	22	87.5
	Repeatability	3.7	5.1	6.2	12.6	36.7
Titanium EB welded plate (Ti-6Al-4 V)	Uncertainty	12.2	15.8	14.5	32.5	298.6
	Repeatability	5.9	7.7	8.3	17.3	130.2
Nickel disk forging (Udimet-720Li)	Uncertainty	20	26.2	21.3	55.5	511.1
	Repeatability	21.5	24.9	29.7	51.7	290.9
Stainless steel forging (304 L)	Uncertainty	44.9	57.1	48.7	132.2	306.6
	Repeatability	20.3	23.8	27.6	52.3	141.3
Stainless steel DM welded plate	Uncertainty	17.5	21.9	19.5	45.5	269.3
	Repeatability	14.9	17.3	21.6	36.3	146.5

The 304L stainless steel forging specimen type is roughly hemi-spherical with an outer diameter of 73.7 mm (2.9 in). They include a forged internal cavity with an inner diameter of 30.5 mm (1.2 in), and a height of 50.8 mm (2.0 in) (Fig. 4). The specimens were produced using a multi-stage forging process. The sample billets were heated to 980 °C (1800 °F) for 60 min, die pressed to 75% of their original height in a hydraulic press, cooled to room temperature, heated to 1750 °F for 60 min, and subjected to a high energy rate

forging operation. The specimens were then cooled to room temperature, annealed at 955 °C (1750 °F) for 30 min, and water quenched. The final processing steps consisted of reheating the specimens to 845 °C (1550 °F) for 60 min, a final high energy rate forging operation, followed by a final water quench.

The nickel based super-alloy (Udimet-720Li) forging specimen had a diameter of 151.20 mm (5.95 in) and a maximum height of 70.41 mm (2.77 in), as shown in

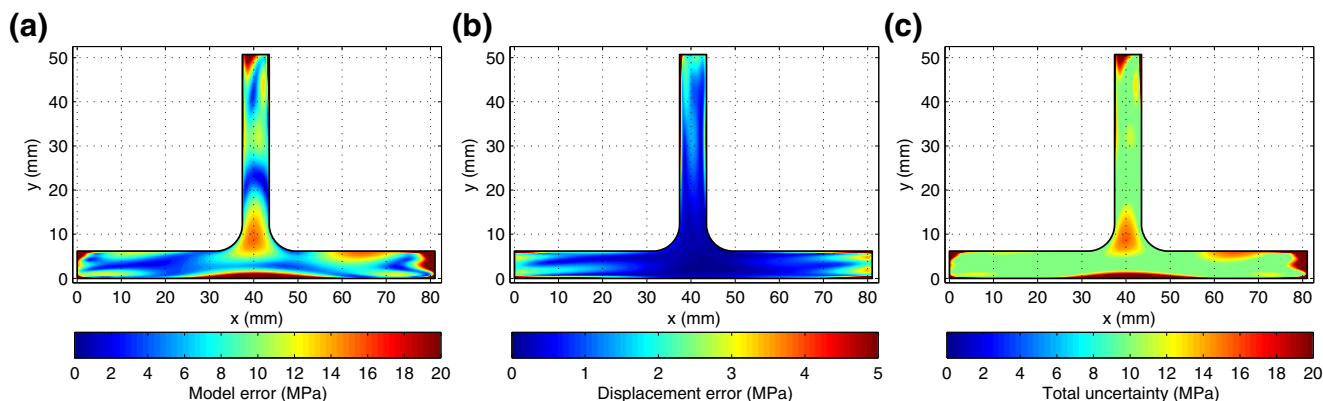


Fig. 7 (a) Displacement error, (b) model error, and (c) total uncertainty for the aluminum T-section specimens



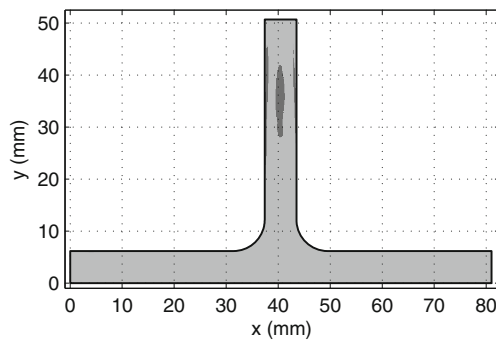


Fig. 8 Diagram of points (95.1%) where the aluminum T-section specimens have a positive (light gray) and negative (dark gray) comparison between uncertainty and precision. Other measurements in the repeatability study met this criterion at 96.8%, 85.3%, 99.2%, 90.1%, 98.7%, 96.2%, 96.5%, 97.9%, and 93.0% of points

Fig. 5. The specimens were forged and heat treated, including a quench, to achieve desired mechanical properties. The heat treatment consisted of pre-heating the specimens to 1080 °C (1975 °F), forging to a nominally finished shape, solution heat treating at 1105 °C (2020 °F), and oil quenching. The specimens were then stabilized at 760 °C (1400 °F) for 8 h, air cooled, aged at 650 °C (1200 °F) for 24 h and then air cooled to room temperature. The forgings were sectioned in half prior to the contour method measurements (to allow for more replicate measurements as discussed in [12]). The stress release from sectioning the forging specimen in half was included in the reported stress values by using a supplemental stress analysis as described in [14]. The stress analysis used measured strain gage data from eight hoop sensing, strain gages placed along the ID and OD of the disk at the subsequent measurement plane (180° from the sectioning plane).

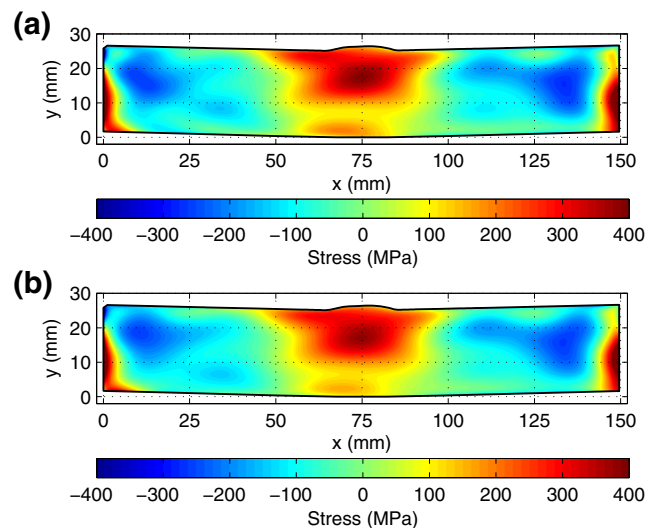


Fig. 10 (a) Measured residual stress (σ_{zz}) and (b) mean of repeatability study for the stainless steel DM welded specimens

Contour Method Measurements

The contour method is a stress-relaxation residual stress measurement technique whose theoretical foundation was established by Prime [15]. A contour method measurement will cut a part along a given measurement plane and surface deformations will occur as a result of residual stress redistribution. The surface profiles at the cut plane can be measured and are analogous to the residual stress before cutting. When the negative of the measured surface profiles are applied as boundary conditions to an elastic finite element model of the part, the residual stress released normal to the cutting plane can be determined. Prime and DeWald [16] have established good practices for experimental steps required for the contour method.

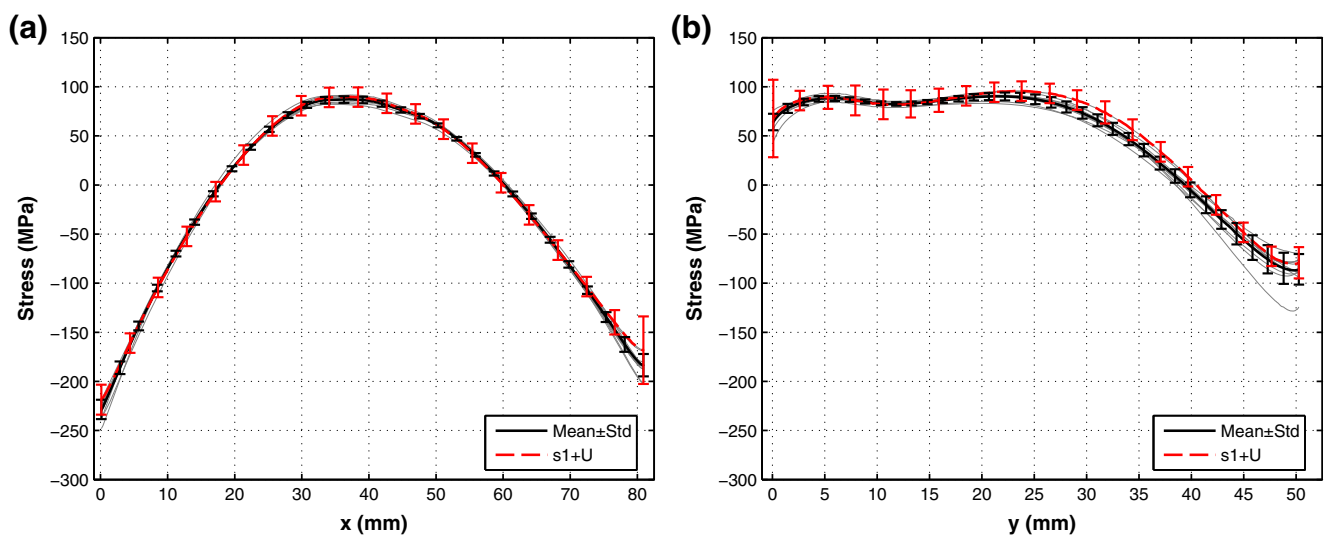


Fig. 9 Line plot of the measured stress with its associated total uncertainty (dashed red) and the repeatability mean (solid black) for the aluminum T-section specimens along the (a) x -direction at $y = 3.18$ mm and (b) along the y -direction at $x = 40.52$ mm. All other measurements are shown with thin gray lines

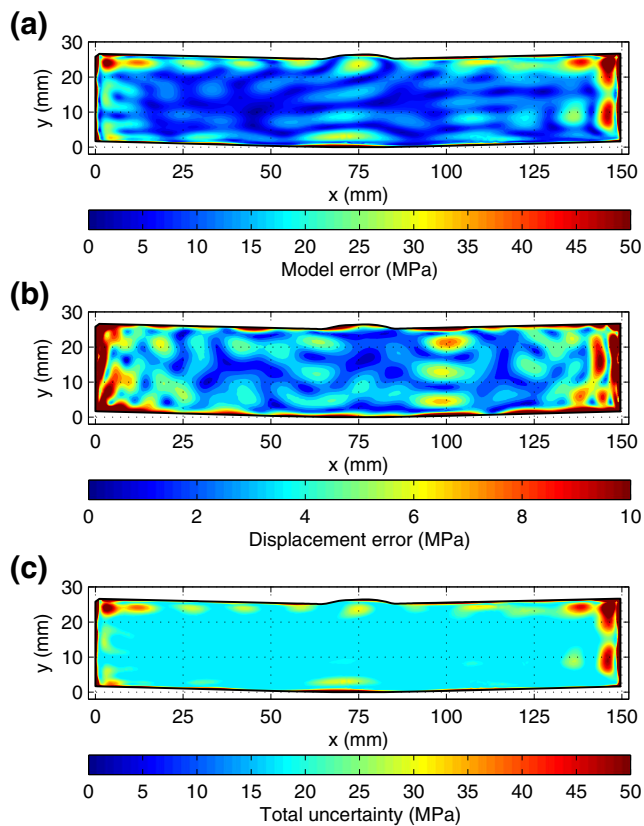


Fig. 11 (a) Displacement error, (b) model error, and (c) total uncertainty for the stainless steel DM welded specimens

Each contour method measurement followed nominally the same procedure. Each specimen was cut in two using wire electric discharge machining (EDM) while rigidly clamped to the EDM tool frame. Following cutting, a laser scanning profilometer was used to measure the surface height profiles normal to the cut plane as a function of in-plane position for each of the two opposing cut surfaces. Surface height data were taken on a grid of points with spacing ranging from 100 to 200 μm in each direction. The two surface profiles were aligned, averaged on a common grid, and fit to a smooth bivariate analytical function. The residual stress release on each measurement plane was determined by applying the negative of the smoothed surface profile as a set of displacement boundary conditions to the cut face of a linear elastic finite

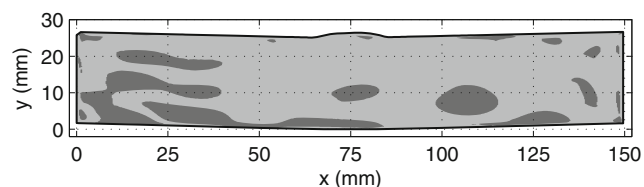


Fig. 12 Diagram of points (80.3%) where the stainless steel DM welded specimens have a positive (light gray) and negative (dark gray) comparison between uncertainty and precision. Other measurements in the repeatability study met this criterion at 72.8%, 73.4%, 67.4%, and 72.4% of points

element model of the cut part. The models used the elastic material properties given in Table 1.

Contour Method Uncertainty Estimation

The uncertainty for each contour method measurement was estimated following the approach outlined in [11]. The uncertainty estimate accounts for two main, random uncertainty sources present in contour method measurements, including the uncertainty associated with random noise in the surface height profiles called the *displacement error* and the uncertainty associated with choosing a specific analytical model to fit the surface profiles called the *model error*.

The displacement error is estimated using a Monte Carlo approach that applied normally distributed noise to the each of the original measured surface height profiles. The normally distributed noise was previously found to approximate the surface roughness that arises from EDM cutting [11]. Stress results were found with five different sets of random noise added to the surface height profiles and the standard deviation of those five residual stress results, at each spatial location, was taken as the displacement error.

The model error is estimated by taking the standard deviation of the residual stress results using displacement surface profiles that have been fit with different analytical models (centered around what was determined to be the best fit). Each case used a different number of fitting coefficients. The total uncertainty was then taken as the root-sum-square of the displacement and model errors with a minimum value of uncertainty set as a floor. The floor used in all cases was the mean of the total uncertainty, which was evaluated over a grid with roughly equal spacing. The uncertainty estimate is assumed to have a normal distribution, which implies that one standard deviation represents a 68% confidence interval.

Comparison of Uncertainty and Precision

The purpose of the single measurement uncertainty estimate is to be able to accurately estimate the random uncertainty that is present during a contour method measurement. To assess whether the uncertainty estimate was accurately estimating random uncertainty, each pointwise measurement result \pm its associated uncertainty was compared with the mean of the repeatability study at the same location. The mean was chosen as the reference value because it is expected to be the most representative of the underlying residual stress field (and the difference between the mean and each measured result is a reasonable representation of the random measurement error, assuming each specimen has a similar initial residual stress state). Every measurement point on the cross-section was assigned to one of two groups depending on whether (positive bin) or not (negative bin) the range of residual stress values at that location defined by the measured stress \pm its associated

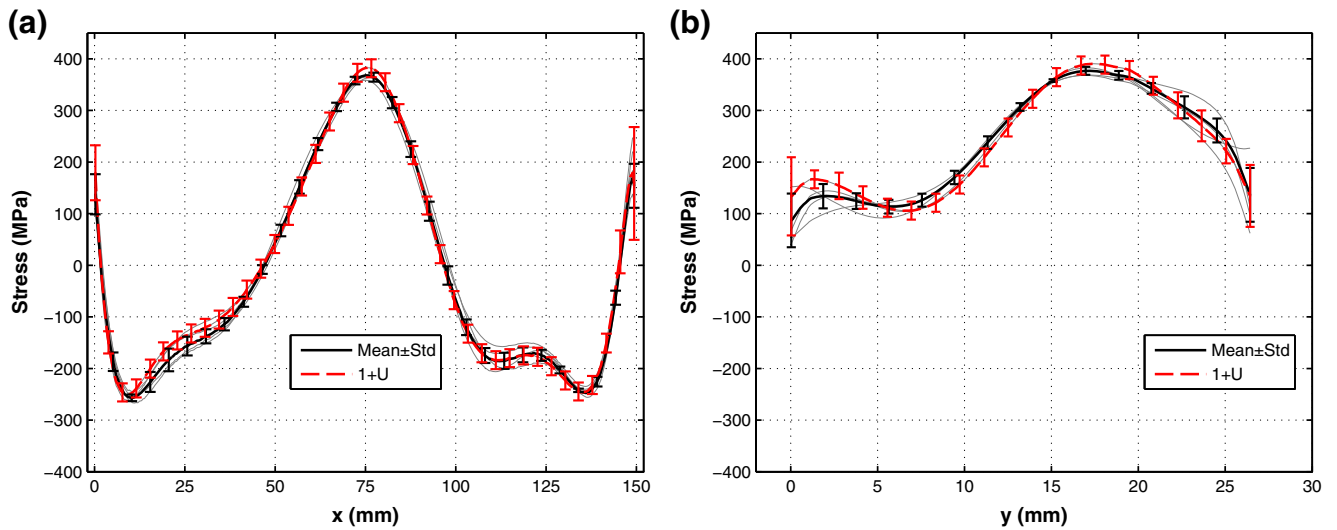


Fig. 13 Line plot of the measured stress with its associated total uncertainty (dashed red) and the repeatability mean (solid black) for the stainless steel DM welded specimens along the (a) x -direction at $y = 19.05$ mm and (b) along the y -direction at $x = 76.2$ mm. All other measurements are shown with thin gray lines

uncertainty included the population mean. Since both uncertainty sources were assumed to have normal distributions, and since the uncertainty estimate is based on one standard deviation, 68% of the points on the cross section are expected to fall within the positive bin.

Results

Results for each of the five specimen conditions are summarized in Fig. 6 through Fig. 26. For each specimen condition the following results are shown: 1) a fringe plot of a typical single measurement result, 2) the estimated uncertainty associated with that measurement result along with the individual contributions to the uncertainty, 3) the mean of each specimen

population, 4) a line plot of residual stress versus position showing each individual measurement, the population mean, and the associated uncertainty for one of the measurements, and 5) a fringe plot showing the locations on the cross-section where the comparison of uncertainty and precision shows a positive or negative result. A summary of tabulated

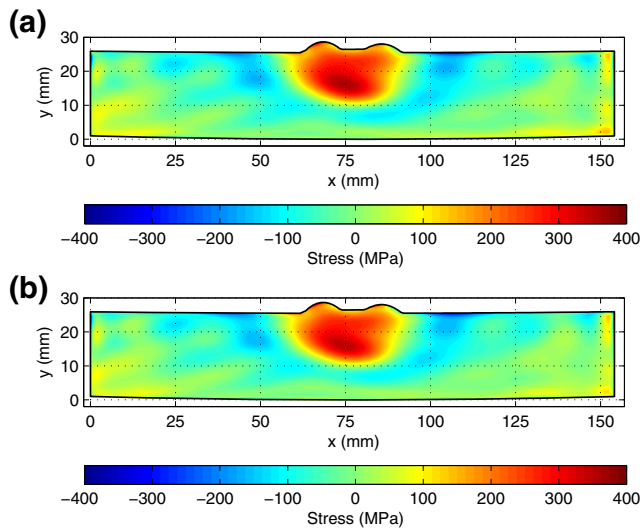


Fig. 14 (a) Measured residual stress (σ_{zz}) and (b) mean of repeatability study for the titanium EB welded plate specimens

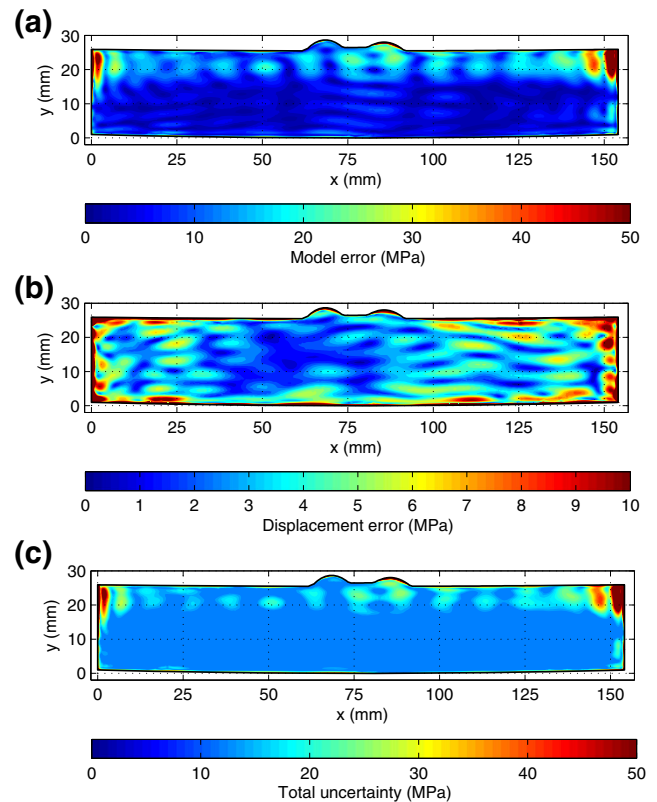


Fig. 15 (a) Displacement error, (b) model error, and (c) total uncertainty for the titanium EB welded plate specimens

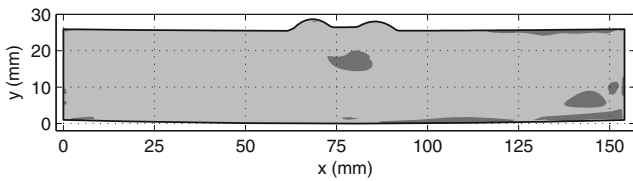


Fig. 16 Diagram of points (94.5%) where the titanium EB welded plate specimens have a positive (light gray) and negative (dark gray) comparison between uncertainty and precision. Other measurements in the repeatability study met this criterion at 97.0%, 92.1%, 98.0%, 98.0%, and 95.7% of points

uncertainty and repeatability standard deviation statistical values for each specimen type is given in Table 2.

Aluminum T-section

The longitudinal stress in the aluminum T-section has compressive stress at the left and right edges of the bottom flange (min \approx

-240 MPa) and at the top of the center flange (≈ -70 MPa) with tensile stress at the intersection of the bottom and center flanges (max ≈ 100 MPa) (Fig. 6(a)). The mean of the population is shown in Fig. 6(b). The uncertainty in the aluminum T-section is shown in Fig. 7. The model error (Fig. 7(a)) is largest along the part boundary (95th percentile is at 21.8 MPa), and at the intersection of the bottom and central flanges. The displacement error (Fig. 7(b)) is also largest along the part boundary (95th percentile is at 3.4 MPa), at the left, right, and top edges. The displacement error is much smaller than the model error. The total uncertainty essentially has the same distribution as the model error (95th percentile is at 22.0 MPa) with a 9.9 MPa floor covering a large portion of the cross-section (Fig. 7(c)).

The comparison between uncertainty and precision was positive at 95.1% of points as shown in Fig. 8 (similar comparisons for the other specimens showed a range of 99.2% to 85.3% and the mean of all specimens is 94.9%).

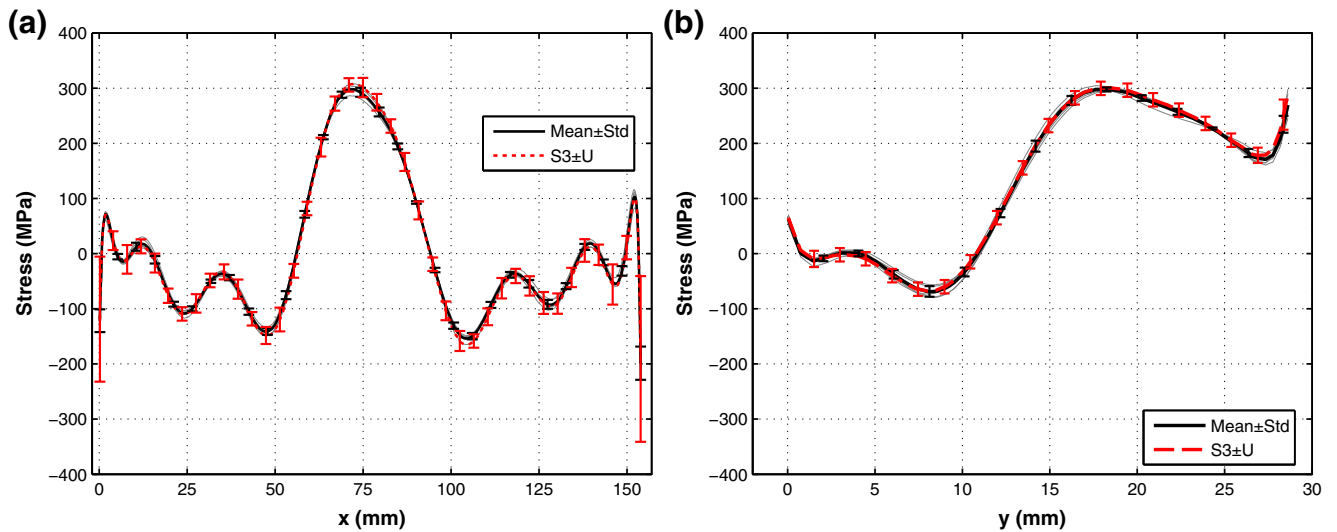
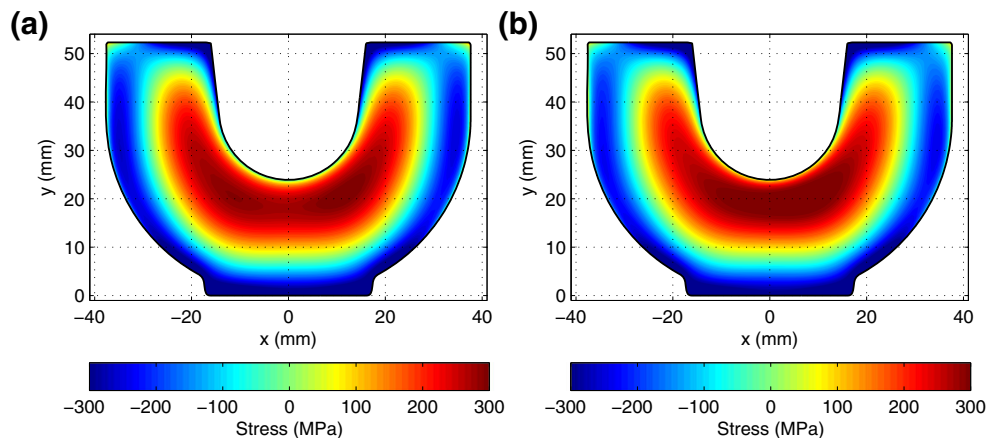


Fig. 17 Line plot of the measured stress with its associated total uncertainty (dashed red) and the repeatability mean (solid black) for the titanium EB welded plate specimens along the (a) x -direction at $y = 20.32$ mm and (b) along the y -direction at $x = 68.15$ mm. All other measurements are shown with thin gray lines

Fig. 18 (a) Measured residual stress (σ_{zz}) and (b) mean of repeatability study for the stainless steel forging specimens



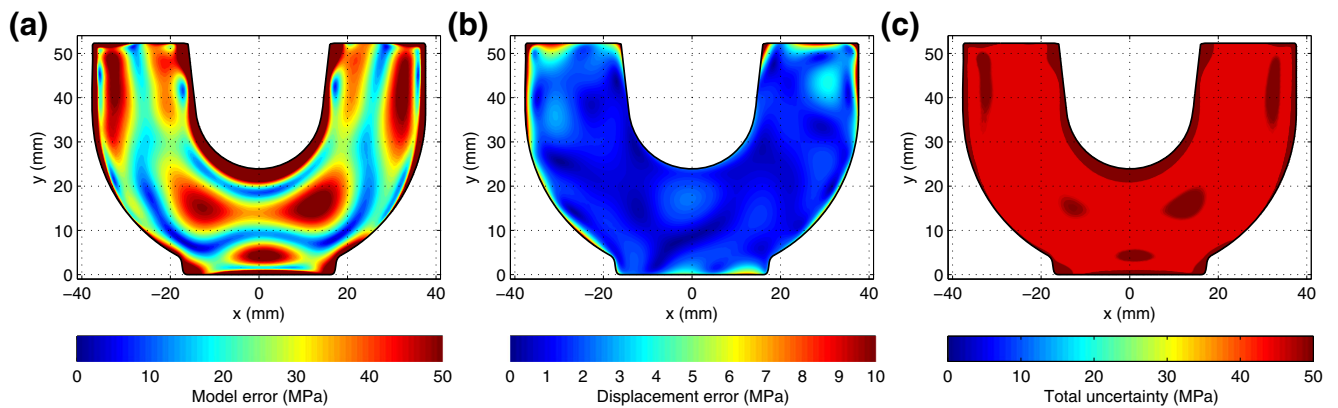


Fig. 19 (a) Displacement error, (b) model error, and (c) total uncertainty for the stainless steel forging specimens

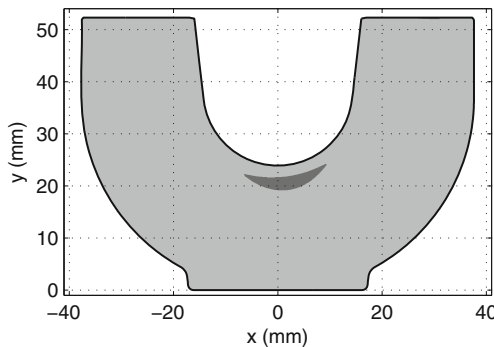


Fig. 20 Diagram of points (99.8%) where the stainless steel forging specimens have a positive (light gray) and negative (dark gray) comparison between uncertainty and precision. Other measurements in the repeatability study met this criterion at 98.8%, 96.6%, 91.4%, and 97.9% of points

Furthermore, the measured residual stress for all repeat measurements along the x -direction at $y = 3.18$ mm and along the y -direction at $x = 40.52$ mm is shown in Fig. 9. The line plots show that the uncertainty estimate

is reasonable at predicting the spread in the measurement data (that is related to random measurement error).

Stainless Steel DM Welded Plate

The longitudinal stress in the stainless steel DM welded plate has tensile stress in the weld area and heat-affected zone (max ≈ 380 MPa) and near $y = 0$ at the left and right edges of the plate where the plate was tack welded (max ≈ 400 MPa). There is compensating compressive stress toward the top of the plate at the left and right edges (min ≈ -260 MPa) (Fig. 10(a), (b)). The uncertainty in the stainless steel DM welded plate is shown in Fig. 11. The model error (Fig. 11(a)) is largest along the part boundary (95th percentile is at 41.0 MPa). The displacement error (Fig. 11(b)) is also largest along the part boundary and at the left, right, and top edges (95th percentile is at 11.8 MPa). The displacement error is much smaller than the model error. The total uncertainty has nearly the same distribution as the model error (95th percentile is at

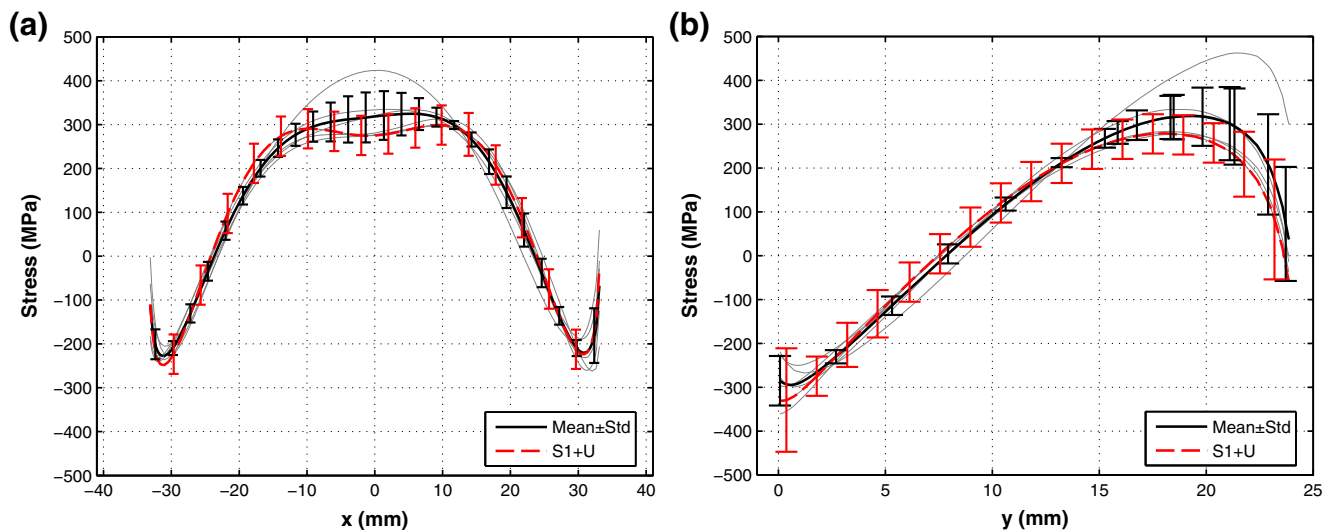


Fig. 21 Line plot of the measured stress with its associated total uncertainty (dashed red) and the repeatability mean (solid black) for the stainless steel forging specimens along the (a) x -direction at $y = 19.05$ mm and (b) along the y -direction at $x = 0$. All other measurements are shown with thin gray lines

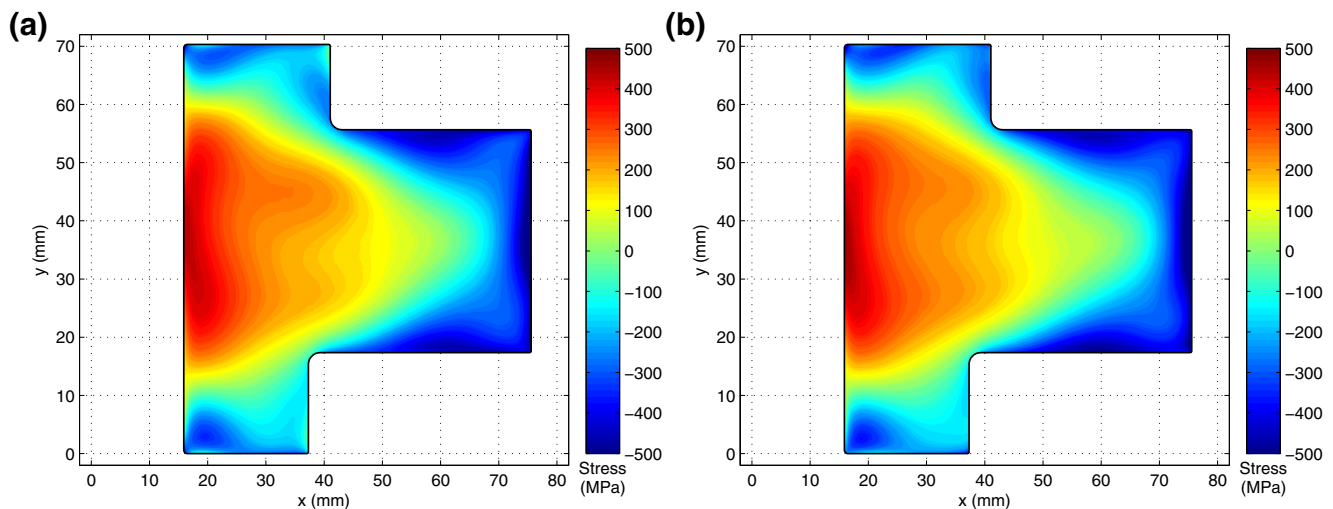


Fig. 22 (a) Measured residual stress (σ_{zz}) and (b) mean of repeatability study for the nickel disk forging specimens

42.5 MPa) with a 17.5 MPa floor covering most of the cross-section (Fig. 11(c)).

The comparison between the uncertainty and precision was positive at 80.3% of points as shown in Fig. 12 (comparisons for the other specimens showed a range of 83.3% to 65.1% and the mean of all specimens is 74.1%). Furthermore, the measured residual stress for all repeat measurements along the x -direction at $y = 19.05$ mm and along the y -direction at $x = 76.2$ mm is shown in Fig. 13. The line plots show that the uncertainty estimate is reasonable at predicting the spread in the measurement data.

Titanium Electron Beam Welded Plate

The longitudinal stress in the titanium EB welded plate has tensile stress in the weld area (max ≈ 350 MPa) and compensating compressive stress in the heat-affected zone (min ≈ -200 MPa) (Fig. 14(a), (b)). The uncertainty in the titanium EB welded plate is shown in Fig. 15. The model error (Fig. 15(a)) is largest along the part boundary (95th percentile is at 27.6 MPa). The displacement error (Fig. 15(b)) is also largest along the part boundary (95th percentile is at 10.8 MPa). As was the case for the other specimens, the displacement error is much smaller than the model error and the total uncertainty mirrors the model error distribution (95th percentile is at 32.5 MPa) with a 12.2 MPa floor covering most of the cross-section (Fig. 15(c)).

The comparison between the uncertainty and precision is positive at 94.5% of points as shown in Fig. 16 (comparison values ranged from 98.0% to 92.1% for the other specimens with a mean of 95.9%). The measured residual stress for all repeat measurements along x -direction at $y = 20.32$ mm and along the y -direction at $x = 68.15$ mm is

shown in Fig. 17. The line plots show that the uncertainty estimate is reasonable at predicting the spread in the measurement data.

Stainless Steel Forging

The hoop stress in the stainless steel forging has tensile stress along the boundary of the forging cavity (max ≈ 340 MPa) and compensating compressive stress around the outer diameter of the forging (min ≈ -260 MPa) (Fig. 18(a)). The measured stress is nominally consistent for five of the six repeat measurements, and the one outlier measurement was omitted from the calculation of the mean (Fig. 18(b)). The outlying measurement had significantly larger stresses near the inner forging cavity (up to 200 MPa larger than the other measurements). The large differences in this measurement were assumed to be primarily related

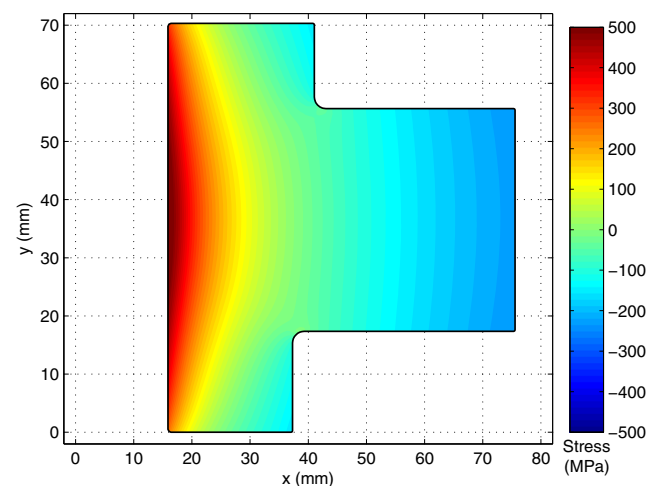


Fig. 23 Stress release when sectioning the nickel disk forging specimens in half

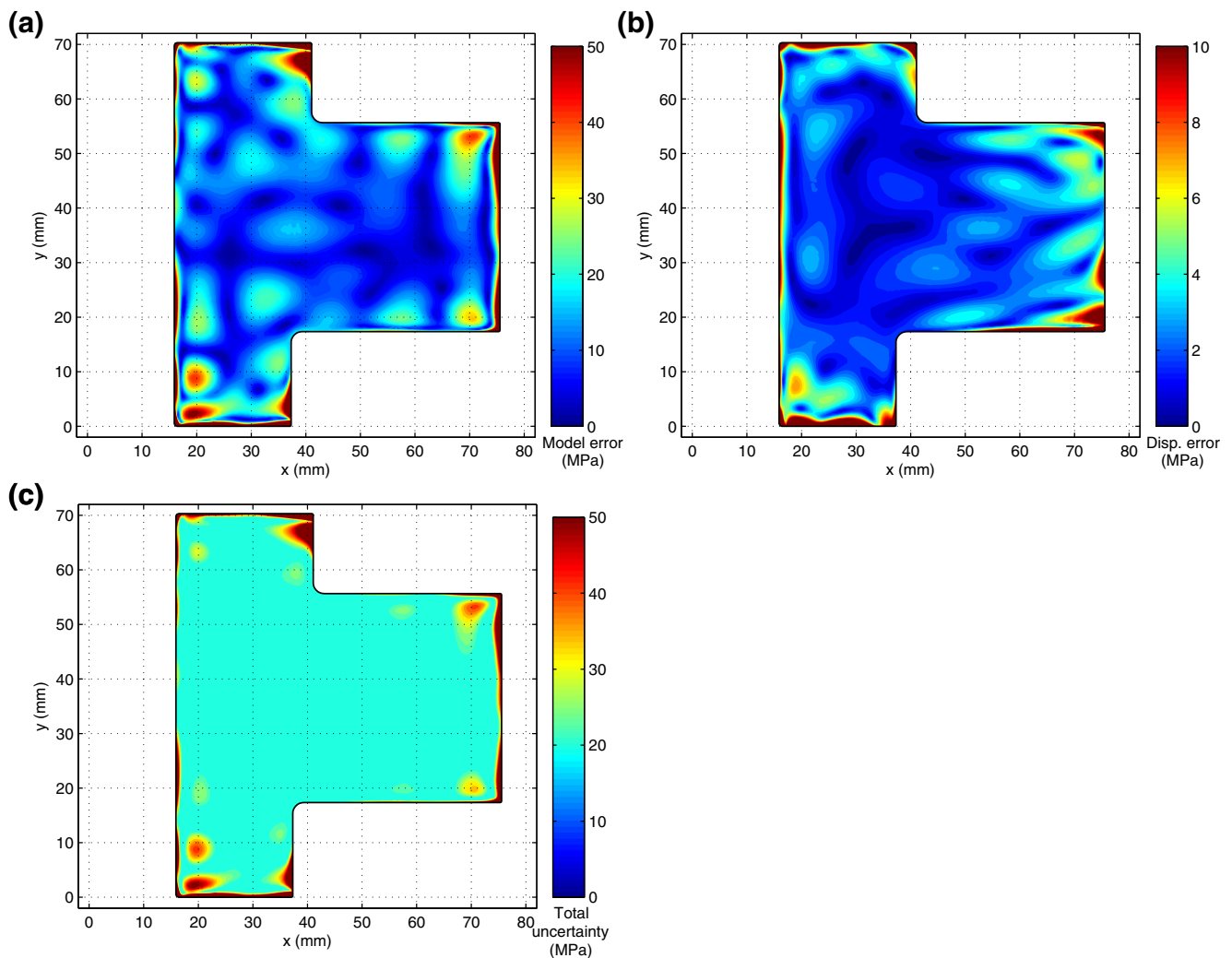


Fig. 24 (a) Displacement error, (b) model error, and (c) total uncertainty for the nickel disk forging specimens

to an inconsistency in the forging process rather than measurement variation, and therefore the outlying result was omitted from the repeatability study. The uncertainty in the stainless steel forging is shown in Fig. 19. The model error (Fig. 19(a)) is largest along the part boundary and is significantly larger than for the other experiments, especially along the boundary of inner forging cavity (95th percentile is at 132.0 MPa). The displacement error (Fig. 19(b)) is also largest along the part boundary (95th percentile is at 6.7 MPa), at the top edges. Consistent with the other cases, the displacement error is much smaller than the model error and the total uncertainty essentially has the same distribution as the model error. The total uncertainty has a 95th percentile at 132.2 MPa and a large 44.9 MPa floor covering most of the cross-section (Fig. 19(c)).

The comparison between the uncertainty and precision was positive at 99.8% of points as shown in Fig. 20 (similar comparisons for the other specimens showed a range of 99.8% to 52.4% and the mean of all specimens is 89.5%). The near totality of points with a positive comparison result is due to

the very large uncertainty floor, which is driven by the high uncertainties at the forging cavity interior. The measured residual stress for all repeat measurements (omitting the outlier) along the x -direction at $y = 19.05$ mm and along the y -direction at $x = 0$ is shown in Fig. 21. The line plots show that the uncertainty estimate conservatively predicts the spread in the measurement data.

Nickel Disk Forging

The hoop stress in the nickel disk forging is tensile towards the center of the forging inner diameter (max ≈ 450 MPa) and has compensating compressive stress toward the forging outer diameter and along the top and bottom of the forging (min ≈ -580 MPa) (Fig. 22(a), (b)). The stress release when sectioning the part in half significantly contributes to the total hoop stress. The sectioning stress has a bending moment type stress distribution with tensile stress towards the ID (max = 550 MPa) and compressive stress towards the OD (min = -230 MPa) (Fig. 23). The uncertainty in the nickel forging is

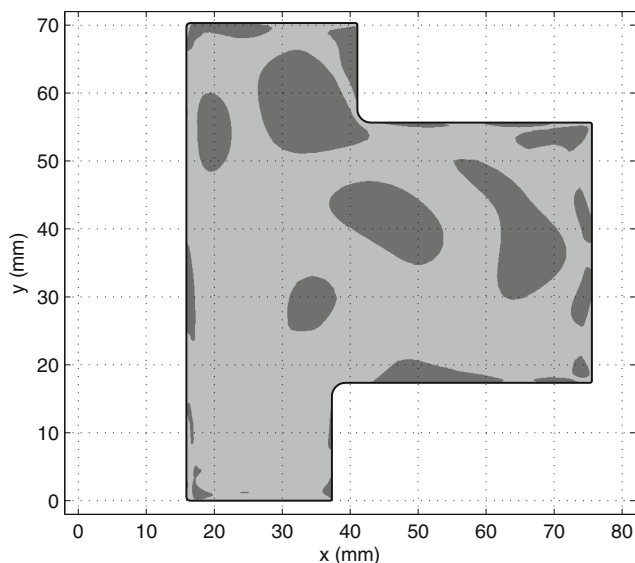


Fig. 25 Diagram of points (76.2%) where the nickel disk forging specimens have a positive (light gray) and negative (dark gray) comparison between uncertainty and precision. Other measurements in the repeatability study met this criterion at 53.0%, 50.0%, 64.8%, 73.1%, and 76.6% of points

shown in Fig. 24. The model error (Fig. 24(a)) is largest along the part boundary (95th percentile is at 54.2 MPa). The displacement error (Fig. 24(b)) is also largest along the part boundary (along the inner and outer diameter as well as the top and bottom edges) (95th percentile is at 11.2 MPa). As was found in the other cases, the displacement error is much smaller than the model error and the total uncertainty is similar to the model error (95th percentile is at 55.5 MPa) with a 20.0 MPa floor covering most of the cross-section (Fig. 24(c)).

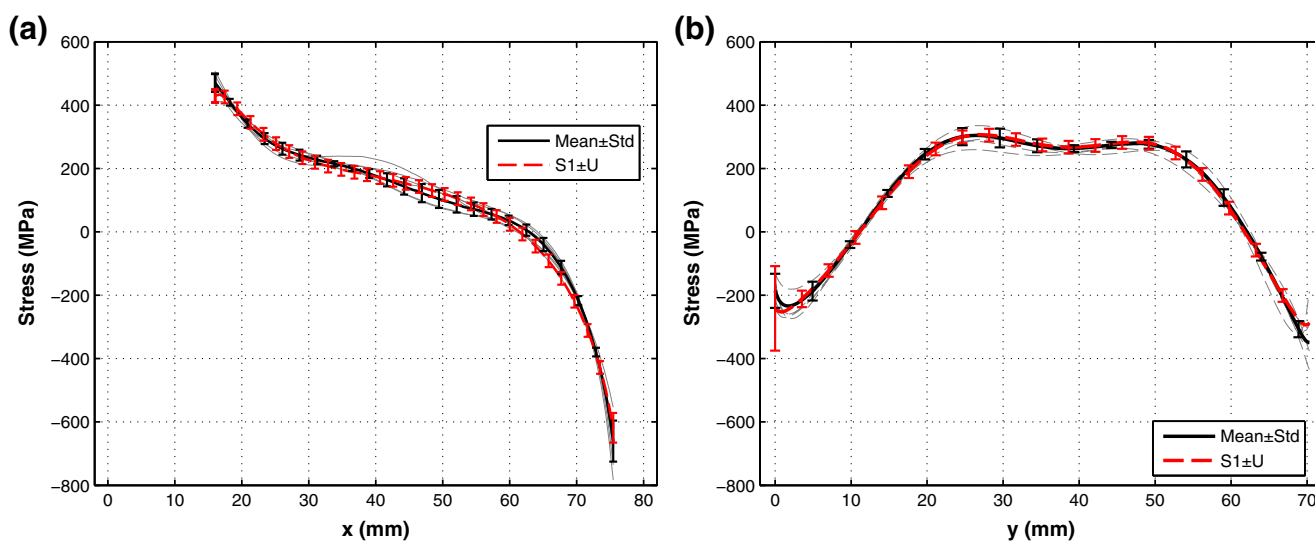


Fig. 26 Line plot of the measured stress with its associated total uncertainty (dashed red) and the repeatability mean (solid black) for the nickel disk forging specimens along the (a) x -direction at $y = 35.15$ mm and (b) along the y -direction at $x = 25.4$ mm. All other measurements are shown with thin gray lines

The comparison between uncertainty and precision was positive at 76.2% of points as shown in Fig. 25 (the comparisons for the other specimens produced positive results at 76.6% to 50.0% and the mean of all specimens is 65.6%). The measured residual stress for all repeat measurements along x -direction at $y = 35.15$ mm and along the y -direction at $x = 25.4$ mm is shown in Fig. 26. The line plots show that the uncertainty estimate reasonably predicts the spread in measurement data.

Discussion

For each case investigated here, the comparison between the uncertainty estimate and the measurement precision produced a positive result at a significantly greater number of points than expected (68%). On average, the comparison was positive at 94.9% of points for the aluminum T-section, 73.3% for the stainless steel DM welded plate, 95.9% for the titanium EB welded plate, 97.0% for the stainless steel forging, and 65.6% for the nickel disk forging. This suggests that the uncertainty estimator is conservative. The estimator is likely to have additional conservatism that stems from real differences among the residual stresses within each population of specimens, since such specimens cannot be made precisely identical, that increases the observed repeatability standard deviation. In summary, the single measurement uncertainty estimator was found to provide a conservative estimate of contour method measurement precision.

Overall, the uncertainty estimate yields similar trends for all cases. Both the model error and the displacement error had spatial distributions with larger uncertainties along the part

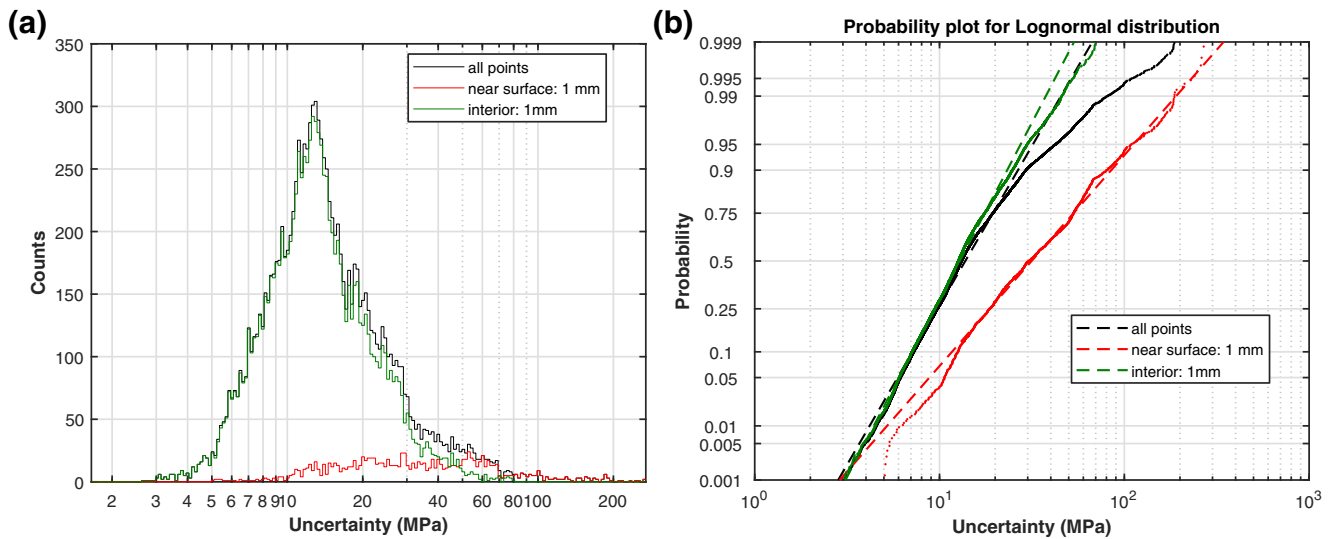


Fig. 27 Uncertainty estimate prior to adding the uncertainty floor for the stainless steel DM welded specimens (a) histogram and (b) probability plot (the dashed lines show a lognormal distribution and the points show the distribution of the data)

boundaries and the displacement error was significantly smaller than the model error. The total uncertainty had nearly the same distribution as the model error, but with most points in the interior having an uncertainty that was determined by the floor.

Histograms of the uncertainty prior to adding the uncertainty floor were created for each case and the histogram for the stainless steel DM welded specimen is shown in Fig. 27(a). The histogram shows that the data roughly follow a log-normal trend and that a portion of the data has large uncertainties. The data were further separated into two groups based on proximity to the perimeter of the cross-section. The near-surface group contained all the points within 1 mm of the part boundary

and the interior group contained the remaining points. The data from each bin were fit to a lognormal distribution as shown in Fig. 27(b) (where the dashed lines show a lognormal distribution and the points show the distribution of the data). The results show that the near-surface points contained most of the high magnitude uncertainties and each data range fits a log-normal distribution reasonably well away from low and high probabilities. Furthermore, when the data are separated into near-surface and interior groups, each fits a log-normal distribution better than did the combined population. Other distances to define the near-surface group were tested (0.5 and 2 mm) and it was found that the results for 1 mm capture most of the high uncertainty points better than using a 0.5 or 2 mm

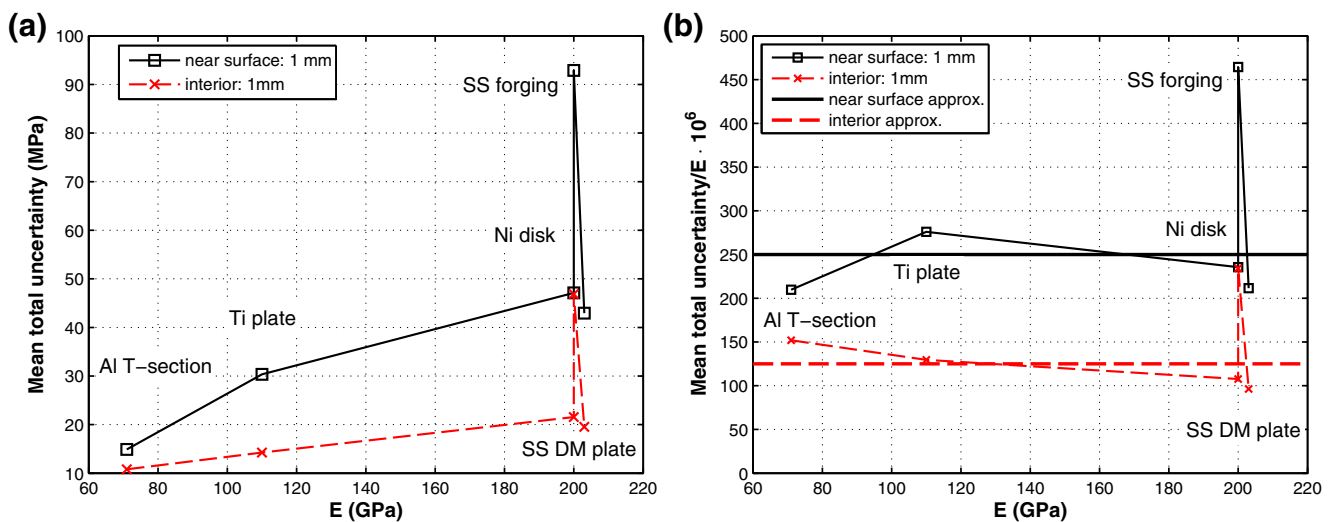


Fig. 28 (a) Line plot of the near surface points (within 1 mm of the part boundary, solid black line) and the interior points (further than 1 mm from the part boundary, dashed red line) of the uncertainty estimate as a function of elastic modulus and (b) normalized by elastic modulus

distance to define the groups. Similar results were found in other specimens, but are not shown for brevity.

Although the trends in uncertainty were similar between cases, the magnitude of the uncertainty estimate was different between the cases. The total uncertainty estimate for near-surface (within 1 mm) and interior points is plotted for each case in Fig. 28(a). When the total uncertainty estimate of the near surface and interior points was normalized by the elastic modulus (Fig. 28(b)) both appear to be nominally constant and follow a trend that can be approximated by $250 \times 10^{-6}E$ for near-surface points and $125 \times 10^{-6}E$ for interior points, where E is the elastic modulus. The stainless steel forging appears to be an outlier, with high uncertainty. We attribute the high uncertainty to areas of high stress magnitude and high stress gradient near the cavity inner wall, which drive up the model error.

The displacement error for all the cases has a minor contribution to the total uncertainty estimate. To quantify the effect of the displacement error on the total uncertainty, the total uncertainty was calculated with and without the displacement error and difference between the floor and 95th percentile was determined for each case. The difference in the floor of the uncertainty estimate with and without the displacement error is 0.1 MPa ($1.4 \times 10^{-6}E$) for the aluminum T-section, 1.0 MPa ($5.0 \times 10^{-6}E$) for the stainless steel DM welded plate, 1.3 MPa ($11.8 \times 10^{-6}E$) for the titanium EB welded plate, 0.1 MPa ($7.0 \times 10^{-6}E$) for the stainless steel forging, and 0.6 MPa ($3.0 \times 10^{-6}E$) for the nickel disk forging. The difference in the 95th percentile of the uncertainty estimate with and without the displacement error is 0.2 MPa ($2.8 \times 10^{-6}E$) for the aluminum T-section, 1.5 MPa ($7.5 \times 10^{-6}E$) for the stainless steel DM welded plate, 4.9 MPa ($44.5 \times 10^{-6}E$) for the titanium EB welded plate, 0.3 MPa ($1.5 \times 10^{-6}E$) for the stainless steel forging, and 1.3 MPa ($6.4 \times 10^{-6}E$) for the nickel disk forging. Since the effect of the displacement error on both the floor and 95th percentile of the total uncertainty estimate was less than 1% of the stress range, the displacement error can be omitted from the uncertainty estimate calculation without a significant impact on the uncertainty estimate. The model error is the larger contributor to the total uncertainty because the analytical models that are used to calculate the model error can change the fit surface displacement profile relatively rapidly as the number of coefficients changes between analytical models, whereas noise in the displacement profiles has a small bearing on the fit profile for a given analytical model.

The dominance of the model error term is interesting and likely also applies in other residual stress measurement methods. In slitting and hole drilling, often the uncertainty is only estimated using a displacement error like estimator (*strain error/uncertainty* in [17]) and omits the *model error/uncertainty* due to the basis functions used in the stress calculation procedure. This could potentially lead to under reported

uncertainties if the model error/uncertainty is significant in those measurement techniques.

Summary/Conclusions

This work compared a recently developed single-measurement uncertainty estimator for the contour method with measurement precision for five experimental conditions. The experimental cases covered a range of specimen geometry, material, and stress condition: an aluminum T-section, a stainless steel plate with a dissimilar metal slot-filled weld, a stainless steel forging, a titanium plate with an electron beam slot-filled weld, and a nickel disk forging. The comparison checked whether the uncertainty estimator enables favorable comparison with the mean stress found from a set of nominally identical repeated measurements. The results of the comparison showed the uncertainty estimate to provide a reasonable approximation of the random uncertainty present in a single contour method measurement. The model error was the largest contributor to the total uncertainty and the displacement error was found to have a negligible contribution. The floor and 95th percentile of the total uncertainty estimate was found to be 9.9 and 22.0 MPa for the aluminum T-section, 17.5 and 41.0 MPa for the stainless steel DM welded plate, 12.2 and 32.5 MPa for the titanium EB welded plate, 44.9 and 132.2 MPa for the stainless steel forging, and 20.0 and 55.5 MPa for the nickel disk forging, respectively. The total uncertainty was found to be related to the elastic modulus with a value of approximately $250 \times 10^{-6}E$ for points within 1 mm of the part boundary and $125 \times 10^{-6}E$ for interior points.

Acknowledgments The authors acknowledge, with gratitude, the U.S. Air Force for providing financial support for this work (contract FA8650-14-C-5026). We would also like to acknowledge Steve McCracken from the Electric Power Research Institute for supplying and fabricating the stainless steel plate with a dissimilar metal slot-filled weld, Thomas Reynolds from Sandia National Laboratory for providing the stainless steel forgings, and Brian Streich from Honeywell for providing the nickel disk forgings.

References

1. ASME (2006) V&V 10–2006: guide for verification and validation in computational solid mechanics. American Society of Mechanical Engineers (ASME), New York
2. Coleman HW, Steele WG (2009) Experimentation, validation, and uncertainty analysis for engineers, 3rd ed. John Wiley & Sons, Inc., Hoboken
3. Smith MC, Smith AC, Wimporoy R, Ohms C (2014/8) A review of the NeT Task Group 1 residual stress measurement and analysis round robin on a single weld bead-on-plate specimen. Int J Press Vessel Pip 120–121:93–140
4. Rathbun HJ, Fredette LF, Scott PM, Csontos AA, Rudland DL (2011) NRC welding residual stress validation program



- international round robin program and findings. In: ASME 2011 pressure vessels and piping conference, pp 1539–1545
5. Tran MN, Hill MR, Olson MD (2015) Further comments on validation approaches for weld residual stress simulation. In: ASME 2015 pressure vessels and piping conference, pp V06BT06A071–V06BT06A071
 6. Hatamleh O (2009/5) A comprehensive investigation on the effects of laser and shot peening on fatigue crack growth in friction stir welded AA 2195 joints. *Int J Fatigue* 31(5):974–988
 7. Hacini L, Van Lê N, Bocher P (2008) Evaluation of residual stresses induced by robotized hammer peening by the contour method. *Exp Mech* 49(6):775
 8. Cuellar SD, Hill MR, DeWald AT, Rankin JE (2012) Residual stress and fatigue life in laser shock peened open hole samples. *Int J Fatigue* 44:8–13
 9. Zhang Y, Fitzpatrick ME, Edwards L (2002) Measurement of the residual stresses around a cold expanded hole in an EN8 steel plate using the contour method. *Mater Sci Forum* 404:527–534
 10. Woo W, An GB, Kingston EJ, DeWald AT, Smith DJ, Hill MR (2013) Through-thickness distributions of residual stresses in two extreme heat-input thick welds: A neutron diffraction, contour method and deep hole drilling study. *Acta Mater* 61(10):3564–3574
 11. Olson MD, DeWald AT, Hill MR, Prime MB (2014) Estimation of uncertainty for contour method residual stress measurements. *Exp Mech* 55(3):577–585
 12. Olson MD, DeWald AT, Hill MR (2018) Repeatability of contour method residual stress measurements for a range of material, process, and geometry. In: Baldi A, Considine J, Quinn S, Balandraud X (eds) *Residual stress, thermomechanics & infrared imaging, hybrid techniques and inverse problems*, vol 8. Conference proceedings of the Society for Experimental Mechanics Series. Springer, Cham
 13. SAE AMS Standard 4342 (2006) Aerospace material specification 4342: aluminum alloy extrusions: solution heat treated, stress relieved, straightened, and overaged. SAE International, Warrendale. <https://doi.org/10.4271/AMS4342>
 14. Wong W, Hill MR (2013) Superposition and destructive residual stress measurements. *Exp Mech* 53(3):339–344
 15. Prime MB (2001) Cross-sectional mapping of residual stresses by measuring the surface contour after a cut. *J Eng Mater Technol* 123(2):162–168
 16. Prime MB, DeWald AT (2013) The contour method. In: Schajer GS (ed) *Practical residual stress measurement methods*. John Wiley & Sons, Ltd, West Sussex, pp 109–138
 17. Prime MB, Hill MR (2006) Uncertainty, model error, and order selection for series-expanded, residual-stress inverse solutions. *J Eng Mater Technol* 128(2):175–185